Supplementary Tables:

Table S1. Source of mouse strains used in the study

Strain	Reference	Our source
Tg:Axin2-d2EGFP	Jho et al., 2002	Tole, S., DBS, TIFR-Mumbai
Mesp1^{Cre}	Saga et al., 1999	Meilhac, S., Institut Imagine, Paris
Tg:Tbx6-Cre	Javali et al., 2017	Generated by us
Tbx6$^{H2B\text{-}EYFP}$	Hadjantonakis et al., 2008	Papaioannou, V., Columbia University Medical Center, New York Stock# 004591
T^{Wis}	Shedlovsky et al., 1988	The Jackson Laboratory, USA Stock# 007676
ROSA^{mTmG}	Muzumdar et al., 2007	The Jackson Laboratory, USA
ROSA^{nlacZ}	Tzouanacou et al., 2009	Tajbakhsh, S., Institut Pasteur, Paris
Myf5^{nlacZ}	Tajbakhsh et al., 1997	Tajbakhsh, S., Institut Pasteur, Paris
Pax7^{GPL}	Sambasivan et al., 2009	Tajbakhsh, S., Institut Pasteur, Paris

Table S2. Small molecules and growth factors

Name	Company	Catalog no.	Concentration
Activin A	R&D	338-AC-050	20 ng/mL
Ascorbic Acid	SIGMA	4403-100MG	0.5 mM
Bmp4	R&D	314-BP-010	10 ng/mL
CHIR99021	Tocris	4423/10	8 μM
Dkk1	R&D	5439-DK-010	150 ng/mL
FGF2	Peprotech	AF-100-18B-100	5-20 ng/mL
Fgf10	R&D	345-FG-025	50 ng/mL
HGF	R&D	2207-HG-025	10 ng/mL
iCRT3	SIGMA	SML0211-5MG	10 μM
iCRT5	Abcam	ab142141	50 μM
IGF-1	Peprotech	250-19-10	2 ng/mL
LDN193189	Stemcell	72142	0.1 μM
SB431542	Tocris	1614/10	10 μM
VEGF	R&D	493-MV-005	5 ng/mL
Xav939	SIGMA	X3004-5MG	5 μM

Table S3. Antibody sources and dilutions

Antigen	Company	Catalog no.	Dilution (IF)	Dilution (WB)	Dilution (FACS)
7-Aminoactinomycin D	ThermoFisher Scientific	A1310			10μg/mL
α-Actinin	SIGMA	A7811	1:200		
β-actin	SIGMA	A5316-.2ML		1:500	
β-catenin	Abcam	ab16051		1:2500	
CD31	BD	550274	1:200		
cardiact TroponinI	Abcam	ab47003	1:120		
cardiac TroponinT	ThermoFisher Scientific	MA5-12960	1:200		
Desmin	SIGMA	D1033	1:40		
Eomes	Abcam	ab23345	1:200		
Flk-1/CD309	ThermoFisher Scientific	12-5821-82			0.5μg / 10^6 cells
GFP	Abcam	ab13970	1:300		
Isl1	DSHB	40.2D6	1:100		
Myod	Dako	M351201-2	1:100		
Myogenin	DSHB	F5D	1:10		
Myosin heavy chain (Skeletal muscle specific)	SIGMA	M4276	1:100		
Nkx2.5	ThermoFisher Scientific	PA5-49431	1:50		
Oct3/4	SantaCruz Biotechnology	sc-8628	3μg/mL		
PDGFRα/CD140a	ThermoFisher Scientific	62-1401-82			1.0μg / 10^6 cells
phospho-Smad2	Cell Signaling Technologies	3108S		1:1000	
Pax3	DSHB	C1-575	1:150		
Sox2	SantaCruz Biotechnology	sc17320	1:67		
Total Smad2/3	Cell Signaling Technologies	5678S		1:1000	
T/Brachyury	SantaCruz Biotechnology	sc-17743	3μg/mL		
Tbx1	Abcam	ab18530	1:100		
Tbx1	ThermoFisher Scientific	PA5-26389	1:100		
Tbx6	Imagenex	custom generated			

Table S4. Mouse RT-qPCR primers

Gene	Primer	Reference
Axin2	AGGAGCAGCTCAGCAAAAAG GCTCAGTCGATCCTCTCCAC	Kurek *et al*, Stem Cell Reports, 2015
Cdx1	GCGTTGGTGGTCTGTGTAGA ACGCCCTACGAATGGATG	qPCR Primer Depot
Cdx2	TCAACCTCGCCACAACCTTCCC TGGCTCAGCCTGGGATTGCT	Rayon *et al*, Dev Cell, 2014
Cdx4	AAATTCCTTTTCCAGCTCCA ATGGATGCGCAAAACTGTG	qPCR Primer Depot
cTnT	CAAGGAGCTGTGGCAGAGTA TTCTGGTTGTCATTGATCCG	Kokkinopoulos *et al*, Dev Dyn, 2015
CYP26a1	AGCTGTTCCAAAGTTTCCATGT ACCCACATGTCCTCCAGAAA	qPCR Primer Depot
Fgf10	GTTGCTGTTGATGGCTTTGA GATTGAGAAGAACGGCAAGG	qPCR Primer Depot
Foxa2	TCATGTTGCTCACGGAAGAG TAAAGTATGCTGGGAGCCGT	qPCR Primer Depot
Hand1	CTTTAATCCTCTTCTCGCCG TGAACTCAAAAAGACGGATGG	qPCR Primer Depot
Isl1	CACGAAGTCGTTCTTGCTGA GGTTAGGGATGGGAAAACCT	Caprio *et al*, PNAS, 2014
Kdr	TCCAGAATCCTCTTCCATGC AAACCTCCTGCAAGCAAATG	qPCR Primer Depot
Lhx2	CCAGCTTCGGACAATGAAGT TTTCCTGCCGTAAAAGGTTG	Harel *et al*, PNAS, 2012
Mixl1	ACTTTCCAGCTCTTTCAAGAGCC ATTGTGTACTCCCCAACTTTCCC	Costello *et al*, Nature Letters, 2011
Mlc2v	AGGGTCACTGAAGGCTGACT GGTCGATCTCCTCTTTGGAG	Kokkinopoulos *et al*, Dev Dyn, 2015
Msc	ACATTCACCCAGTCAACCTG CCACTTCCTTCAGGTCATTCTC	Sambasivan *et al*, Dev Cell, 2009
Msgn1	CTCTGCTTTTCCAGTCCCAG AACCTGGGTGAGACCTTCCT	qPCR Primer Depot
Myf5	GACAGGGCTGTTACATTCAGG TGAGGGAACAGGTGGAGAAC	qPCR Primer Depot
MyoD	GTCGTAGCCATTCTGCCG AGCACTACAGTGGCGACTCA	qPCR Primer Depot
MyoG	GTGGGAGTTGCATTCACTGG CTACAGGCCTTGCTCAGCTC	qPCR Primer Depot
Nanog	AAAGGATGAAGTGCAAGCG TCTGGCTGCTCCAAGTT	Kurek *et al*, Stem Cell Reports, 2015
Nkx2.5	AAGCAACAGCGGTACCTGTC GCTGTCGCTTGCACTTGTAG	Shelton *et al*, Stem Cell Reports, 2014

Oct4	GAACATGTGTAAGCTGCGG CAGACTCCACCTCACACG	Kurek *et al*, Stem Cell Reports, 2015
Otx2	GAAAATCAACTTGCCAGAATCCA GCGGCACTTAGCTCTTCGAT	Iwafuchi-Doi, Development, 2012
Pitx2	TGTCCACTCGCGAAGAAATC AAGCCATTCTTGCACAGCTC	Sambasivan *et al*, Dev Cell, 2009
RALDH2	GCTCTCCTGTGGCTGGATTA GCCCAACCTCGAGATCAAGT	qPCR Primer Depot
Sox17	TCTTGGGGAAATAGGAAGGC TGGAACCTCCAGTAAGCCAG	qPCR Primer Depot
Sox2	AGCTCGCAGACCTACATGAA CCCTGGAGTGGGAGGAA	Kurek *et al*, Stem Cell Reports, 2015
T/Bra	CATGTACTCTTTCTTGCTGG GGTCTCGGGAAAGCAGTGGC	Lolas *et al*, PNAS, 2014
Tbx1	TGTGGGACGAGTTCAATCAG TGTCATCTACGGGCACAAAG	Sambasivan *et al*, Dev Cell, 2009
Tbx1 (Set 2)	CATGAGCAGCATGTAGTCGG TGTGGGACGAGTTCAATCAG	qPCR Primer Depot
Tbx5	TGGTTGGAGGTGACTTTGTG GGCAGTGATGACCTGGAGTT	qPCR Primer Depot
Tbx6	GTGTATCCCCACTCCCACAG CCGAGAAAATGGCAGAAACT	qPCR Primer Depot
Tcf21	CTGTAGTTCCACACAAGCGG CGGTTACATTCACCCAGTCA	qPCR Primer Depot

Table S5. Human RT-qPCR primers

Gene	Primer	Reference
Axin2	CTGGTGCAAAGACATAGCCA AGTGTGAGGTCCACGGAAAC	qPCR Primer Depot
Isl1	CGCATTTGATCCCGTACAAC GGTTTCTCCGGATTTGGAAT	Harel *et al*, PNAS, 2012
Mixl1	CCGAGTCCAGGATCCAGGTA CTCTGACGCCGAGACTTGG	Mendjan *et al*, Cell Stem Cell, 2014
Msgn1	AGAGGGAGAAGCTCAGGATGAG GTGTCTGGATCTTGGTGAGAGG	qPCR Primer Depot
Nanog	TTGGGACTGGTGGAAGAATC GATTTGTGGGCCTGAAGAAA	qPCR Primer Depot
Nkx2.5	AGCTCATAGACCTGCGCCT AGGACCCTAGAGCCGAAAAG	qPCR Primer Depot
Oct4	CTGGTTCGCTTTCTCTTTCG CTTTGAGGCTCTGCAGCTTA	qPCR Primer Depot
Otx2	GCTGTTGTTGCTGTTGTTGG AGAGGAGGTGGCACTGAAAA	qPCR Primer Depot
Sox2	GGAAAGTTGGGATCGAACAA GCGAACCATCTCTGTGGTCT	qPCR Primer Depot
T/Bra	TATGAGCCTCGAATCCACATAGT CCTCGTTCTGATAAGCAGTCAC	qPCR Primer Depot
Tbx1	CAGCTTTCACTTCCTTGTCCT ACCCTGAGGACTGGCCC	Harel *et al*, PNAS, 2012
Tbx6	AGCCTGTGTCTTTCCATCGT GCTGCCCGAACTAGGTGTAT	Mendjan *et al*, Cell Stem Cell, 2014
Tcf21	TTCAGGTCACTCTCGGGTTT AGCTACATCGCCCACTTGAG	Harel *et al*, PNAS, 2012
Twist1	TCCATTTTCTCCTTCTCTGGAA GGCTCAGCTACGCCTTCTC	qPCR Primer Depot

Supplementary Figures:

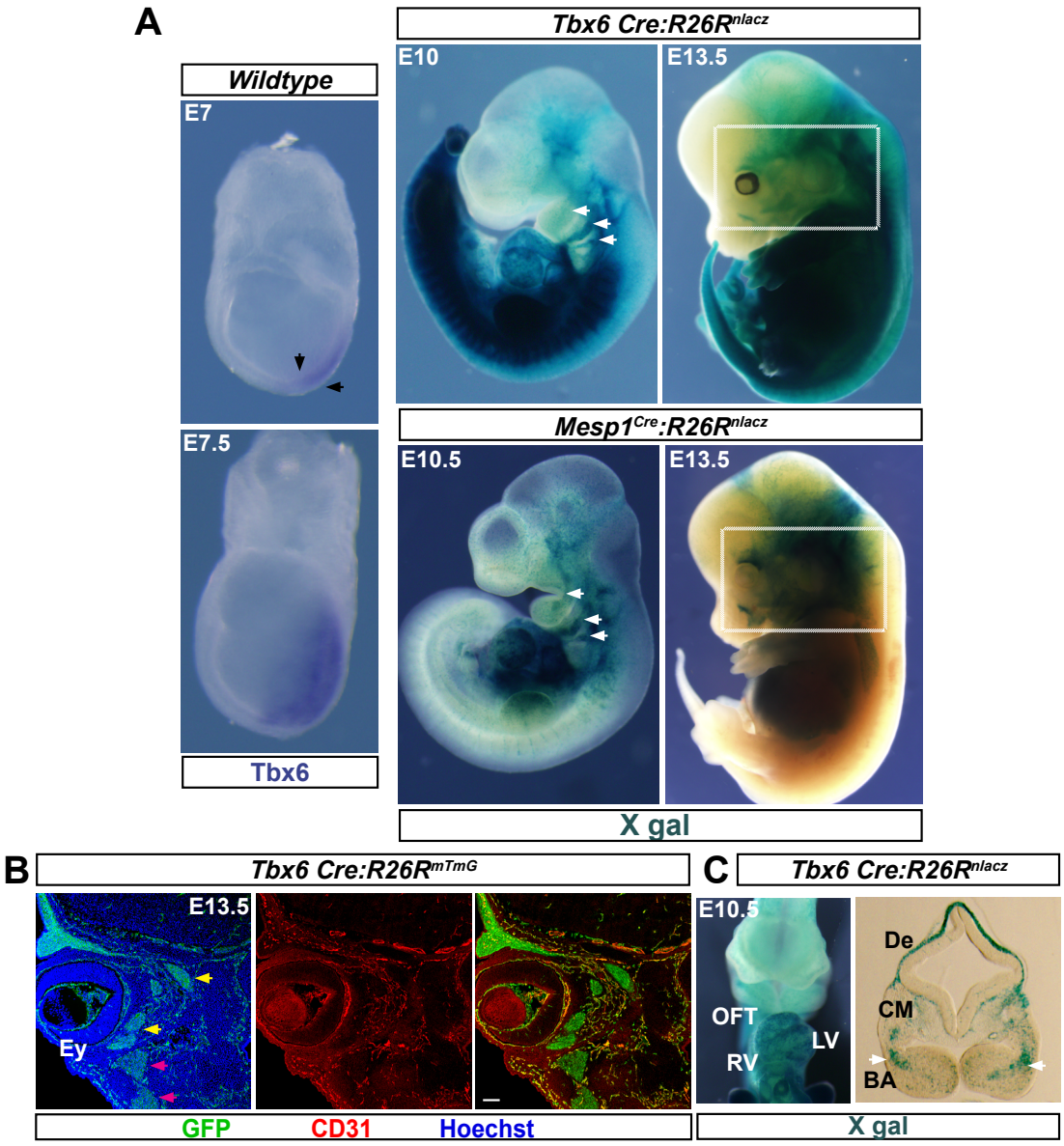

Figure S1: *Tbx6*-lineage trace marks head mesoderm including its head muscle derivatives. A) Wholemount ISH (left) on gastrulating mouse embryos. Black arrows, anterior primitive streak. Note, expression in the anterior primitive streak, the source of head mesoderm progenitors. Right panel shows X-gal stained littermates. White arrows, pharyngeal arch-derived muscles; White box highlights head mesoderm derivatives. *Mesp1*^{Cre} serves as an example of head mesoderm lineage reporter. B) Immunostaining of a coronal sections of E13.5 head. Note, *Tbx6-Cre* mediated GFP expression in extraocular (yellow arrows) as well as 1st and 2nd arch muscle progenitors (pink arrows). CD31 co-staining reveals endothelia marked by *Tbx6*-lineage. Scale bar 50 µm. C) *Tbx6-Cre* also marks the anterior-most mesoderm, heart, including the first (left ventricle, LV) and second heart field derivatives (Outflow tract, OFT; right ventricle, RV). Repeats are at least 3 embryos and 2 litters.

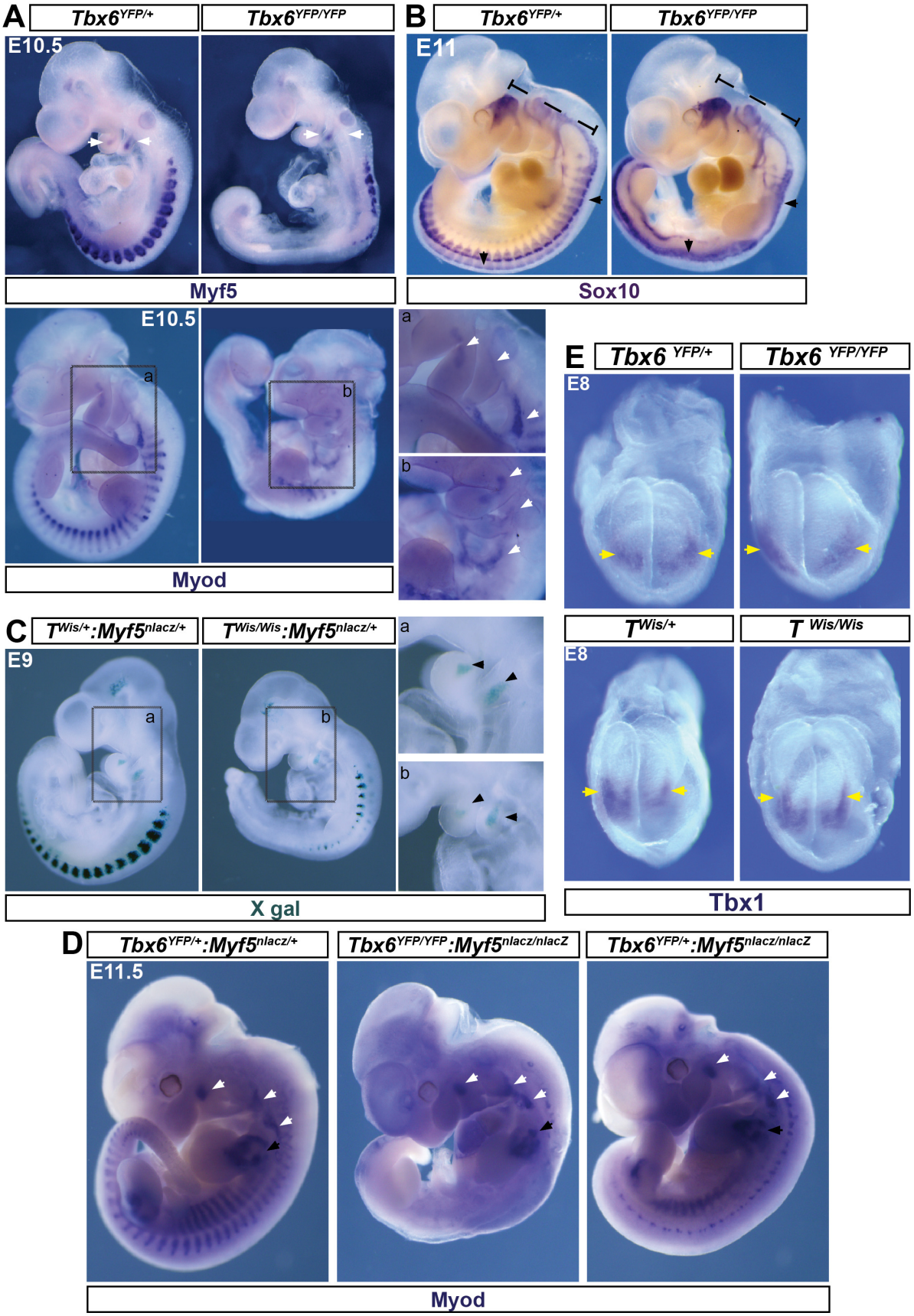

Figure S2: *T* and *Tbx6* dispensable for head mesoderm and head muscle development unlike that of posterior somitic mesoderm. A) ISH of littermate embryos. Since neural crest patterning is mesoderm-dependent, neural crest gene *Sox10* serves as an indirect marker of mesoderm development. *Sox10* reveals severe failure to pattern dorsal root ganglia from trunk neural crest (black arrows), while head mesoderm-dependent cranial ganglia appears to pattern and develop normally (dashed line). Note, although the cervical somites are formed in the mutants, the dorsal root ganglia from the neural crest are not patterned. For all ISH, n = 3 mutant embryos, at least. B) ISH of littermate embryos. *Myf5* RNA expression correlates with *Myf5* reporter expression data shown in Figure 1. ISH for *Myod* shows unperturbed progression in myogenic lineage in the pharyngeal arches (white arrowheads). C) Wholemount X gal staining of littermate embryos. No apparent delay in induction of *Myf5* reporter in the pharyngeal arches (black arrowheads). Note, *T* as well as *Tbx6* null mutants shown in A and C are slightly developmentally delayed compared to heterozygous littermates. Accounting for this age difference, the induction of *Myf5* reporter and *Myod* in arch muscle progenitors in mutants appear comparable to that in heterozygote or wildtype controls. D) ISH for *Myod* shows unperturbed progression in myogenic lineage in the pharyngeal arches (white arrowheads) in double nulls compared to age-matched controls. Note, the muscle anlage in the forelimb (black arrowheads) are also formed as in control embryos suggesting unaffected development of migratory muscle progenitors from cervical somites. E) ISH shows unperturbed *Tbx1* induction in a subset of early head mesoderm (yellow arrowheads).

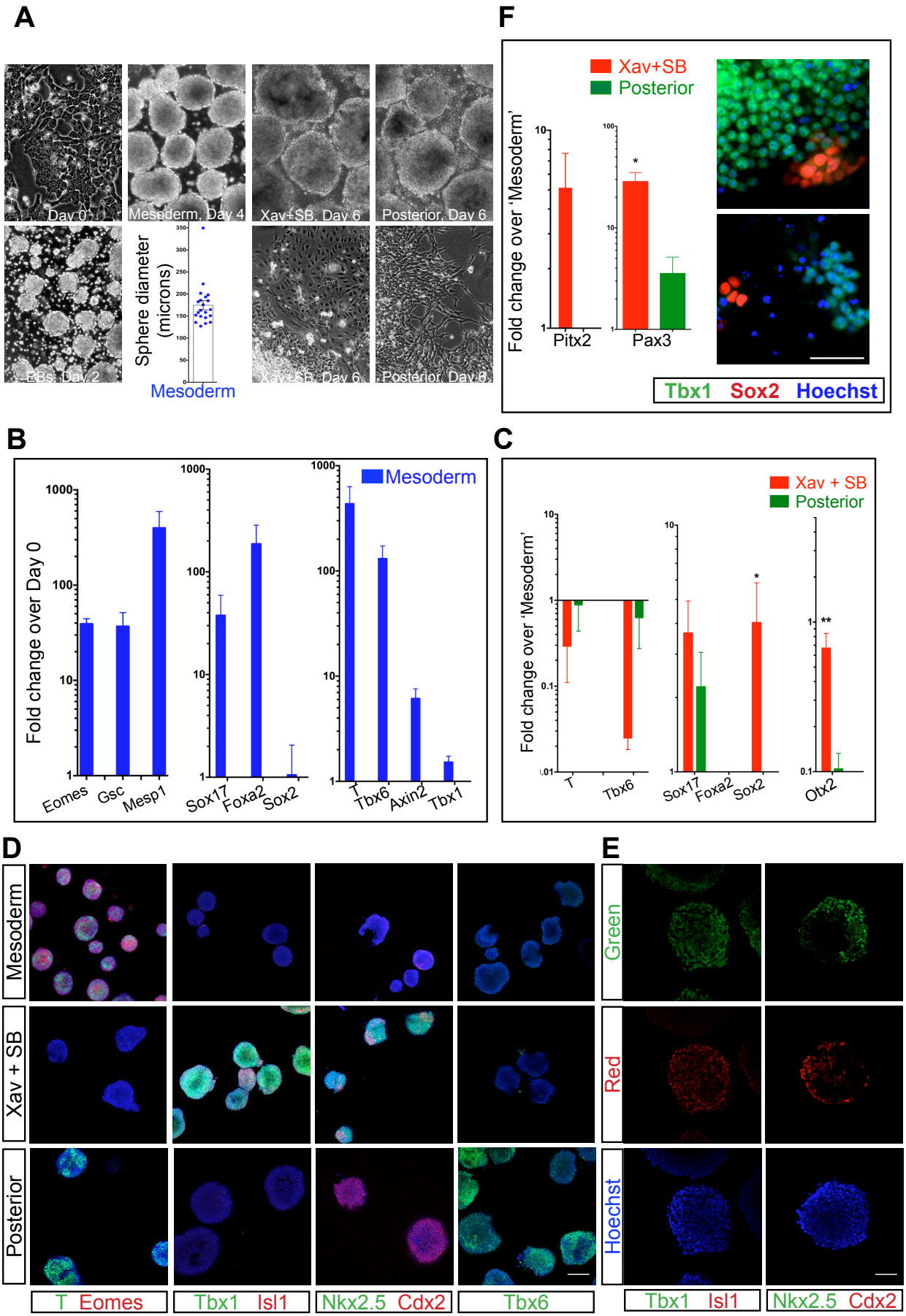

Figure S3: Inhibition of Wnt and Nodal in cardiopharyngeal mesoderm marker induction.
A) Micrographs of cultures during the course of differentiation. The panels show embryoid bodies (EBs) and differentiated spheres derived from EBs. The last two panels in the bottom row show corresponding adherent cultures plated on Day 4.
Diameter of Mesoderm spheres in microns: 174.7 ± 10.4 (mean ± SEM). n=21 spheres.
B) RT-qPCR analysis for early anterior streak markers (Eomes, Gsc, Mesp1), endoderm (Sox17, Foxa2), neurectoderm (Sox2) and mesoderm (T, Tbx6) markers in 'Mesoderm' condition over Day0. Induction of Wnt pathway is inferred by Axin2 expression.
C) RT-qPCR analysis for mesoderm (T, Tbx6), endoderm (Sox17, Foxa2), neurectoderm (Sox2) and anterior (Otx2) markers at Xav+SB or Posterior, when compared to 'Mesoderm'.
D) View of a larger field of the immunostaining assay. Oct4, pluripotency marker. T, Eomes, mesoderm markers. Tbx1, Isl1, Nkx2.5 cardiopharyngeal mesoderm markers. Tbx6, Cdx2, posterior mesoderm markers. Scale bars 200 μm.
E) Split channel view of CPM markers (Tbx1, Isl1, Nkx2.5) and Posterior marker Cdx2 at Xav+SB. For merged image see Fig. 4B. Scale bar 50 μm.
F) RT-qPCR data shows induction of Pitx2 and Pax3 in Xav+SB. In the mouse embryos, initially *Pitx2* marks premandibular mesoderm, but is induced later in somites as well (L'Honore et al., 2010). Though not statistically significant, we observed *Pitx2* induction in dual inhibition (Xav+SB; Figure S3E) cultures. Nevertheless, owing to lack of specific markers, premandibular mesoderm identity upon dual inhibition could not be ascertained. Consistent with the upregulation of *Sox2* RNA (Figure S3C), immunofluorescence assay shows Sox2+ neural clusters negative for Tbx1. Nearly 20% of the spheres in Xav+SB cultures had a few small clusters positive for Sox1+ (another neural marker; not shown). Pax3 protein was undetectable in these cultures (not shown). Mean values from 3 biological replicates plotted; error bars are SEM; p value calculated by Student's t test, unpaired; * < 0.05; Scale bar 50 μm.

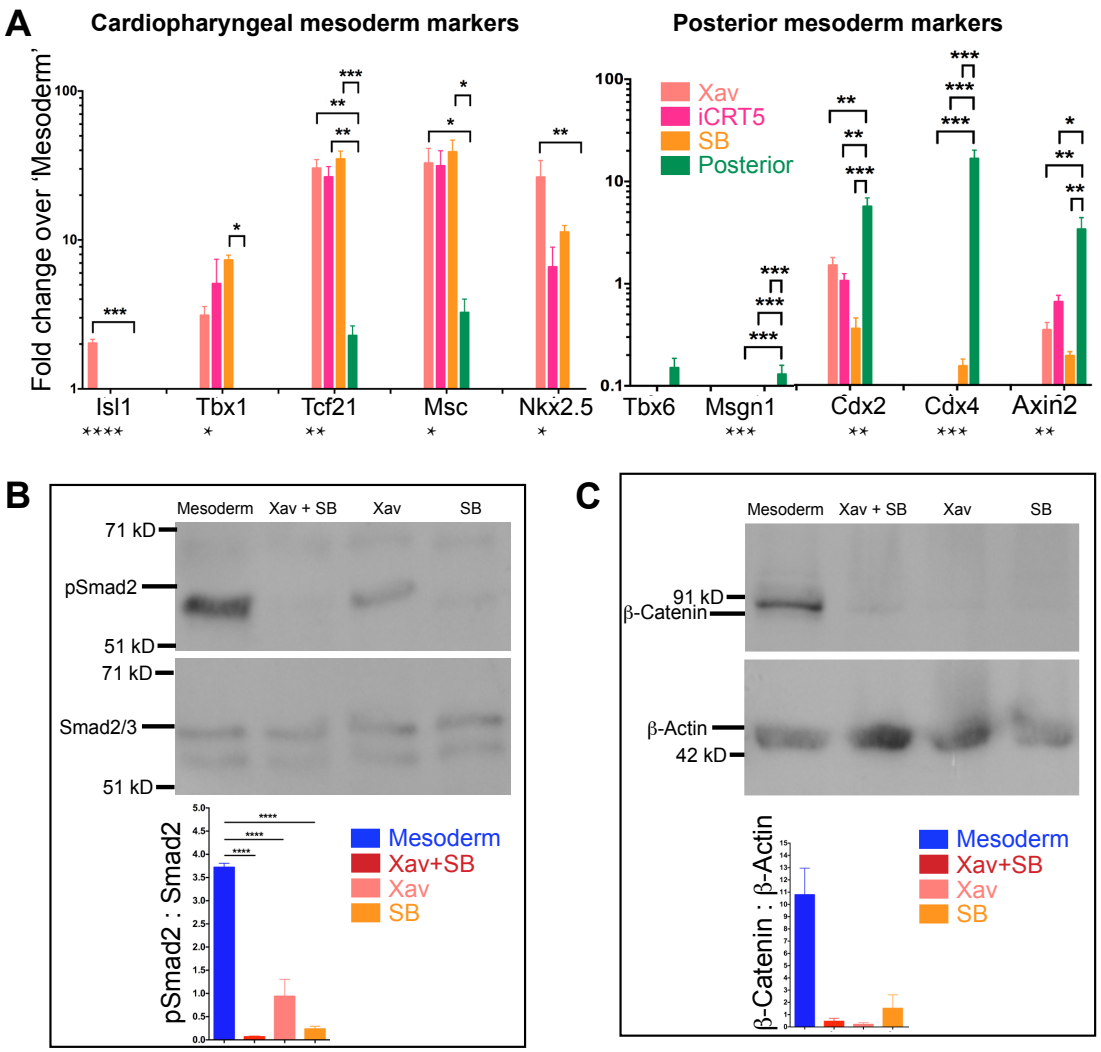

Figure S4: Cardiopharyngeal mesoderm marker induction in mESC-derived mesoderm by inhibition of Wnt and/or Nodal.

A) RT-qPCR analysis for marker genes comparing treatments with Wnt antagonist Xav 939 alone (Xav), Wnt/**β**-catenin transcription response inhibitor iCRT5 alone, Nodal inhibitor SB alone and 'Posterior'. Mean values from 3 biological replicates have been plotted; error bars are SEM; p value calculated by One-way ANOVA is indicated below X-axis. Dunnett's post hoc test was performed by pairwise comparison of individual inhibitor treatment to 'Posterior'. The significance in p value by ANOVA is indicated below X-axis and that of Dunnett's above the bars. * < 0.05, ** <0.01, *** <0.001 and so on.

B) Immunoblot shows reduced phospho-Smad 2 (p-smad2) levels verifying diminished Nodal signaling upon treatment with Xav+SB, Xav alone and SB alone. Molecular weight marker positions are indicated on the left. Histogram indicates levels of phospho-Smad2 normalized to total Smad2. For all histograms, mean values from biological triplicates have been plotted; error bars are SEM; p value calculated by One-way ANOVA is indicated below X-axis. Tukey's post hoc test was performed for pairwise comparisons of individual inhibitor treatments. n=3 experiments. The significance in p value by Tukey's is indicated above the bars. * < 0.05, ** <0.01, *** <0.001, **** <0.0001 and so on.

C) Immunoblot shows reduced β-catenin levels verifying diminished Wnt signaling upon treatment with Xav+SB, Xav alone and SB alone. Molecular weight marker positions are indicated on the left. Histogram indicates levels of β-catenin with respect to β-Actin. For all histograms, mean values from biological duplicates have been plotted; error bars are SEM. n=2 experiments.

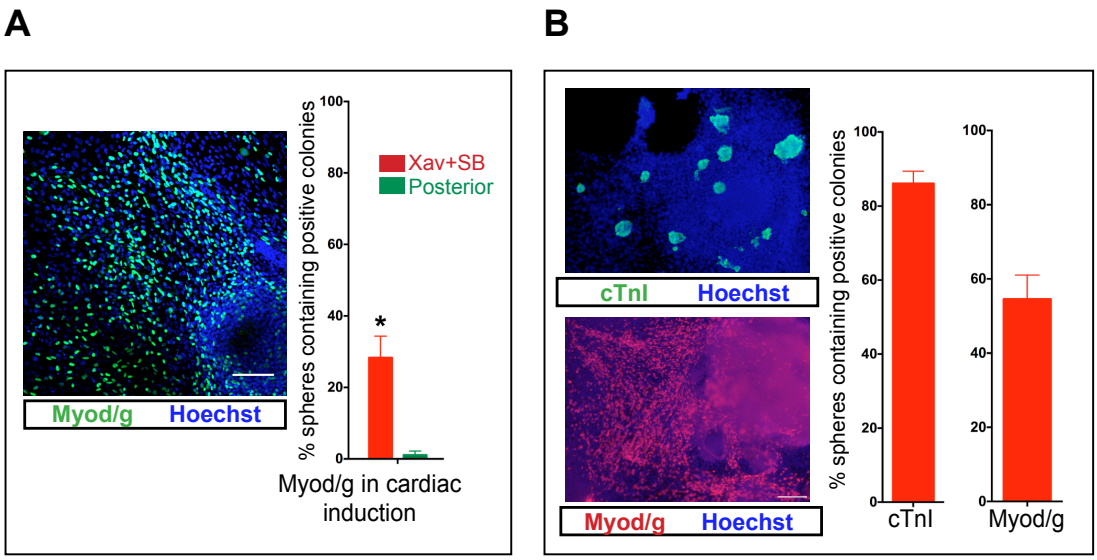

Figure S5: Dual differentiation potential of *in vitro* CPM-like population.
A) Immunostaining shows skeletal muscle differentiation in cardiogenic culture condition. Proportion of spheres associated with Myod/Myog positive clusters in cardiogenic cultures is 28.3 ± 6% (mean ± SEM) in Xav+SB-derived and 1.1 ± 1.1% in 'Posterior' derived cultures. Mean values from 3 biological replicates plotted; error bars are SEM; p value calculated by Student's t test, unpaired; * < 0.05; ** < 0.01; scale bar 100 μm.
B) Immunostaining shows skeletal and cardiac muscle differentiation from another mESC line (B6D2) when Xav+SB cells were differentiated in N2B27 containing media. Proportion of spheres associated with cardiac TroponinI positive clusters is 86.1 ± 3.3% (mean ± SEM) and proportion of spheres associated with Myod/Myog positive clusters is 54.5 ± 6.5%. Mean values from 6 biological replicates plotted; error bars are SEM; scale bar 50 μm.

Supplementary References:

Caprio, C. and Baldini, A. (2014). p53 suppression partially rescues the mutant phenotype in mouse models of DiGeorge syndrome. *Proc. Natl. Acad. Sci.* **111**, 13385–13390.

Costello, I., Pimeisl, I.-M., Dräger, S., Bikoff, E. K., Robertson, E. J. and Arnold, S. J. (2011). The T-box transcription factor Eomesodermin acts upstream of Mesp1 to specify cardiac mesoderm during mouse gastrulation. *Nat. Cell Biol.* **13**, 1084–1091.

Hadjantonakis, A. K., Pisano, E. and Papaioannou, V. E. (2008). Tbx6 regulates left/right patterning in mouse embryos through effects on nodal cilia and perinodal signaling. *PLoS One* **3**, e2511.

Harel, I., Maezawa, Y., Avraham, R., Rinon, A., Ma, H.-Y., Cross, J. W., Leviatan, N., Hegesh, J., Roy, A., Jacob-Hirsch, J., et al. (2012). Pharyngeal mesoderm regulatory network controls cardiac and head muscle morphogenesis. *Proc. Natl. Acad. Sci.* **109**, 18839–18844.

Iwafuchi-Doi, M., Matsuda, K., Murakami, K., Niwa, H., Tesar, P. J., Aruga, J., Matsuo, I. and Kondoh, H. (2012). Transcriptional regulatory networks in epiblast cells and during anterior neural plate development as modeled in epiblast stem cells. *Development* **139**, 4675–4675.

Javali, A., Misra, A., Leonavicius, K., Acharyya, D., Vyas, B. and Sambasivan, R. (2017). Co-expression of Tbx6 and Sox2 identifies a novel transient neuromesoderm progenitor cell state. *Development* **144**, 4522–4529.

Jho, E., Zhang, T., Domon, C., Joo, C., Freund, J. and Costantini, F. (2002). Wnt / β -Catenin / Tcf Signaling Induces the Transcription of Axin2 , a Negative Regulator of the Signaling Pathway Wnt / ß-Catenin / Tcf Signaling Induces the Transcription of Axin2 , a Negative Regulator of the Signaling Pathway. *Mol. Cell. Biol.* **22**, 1172–1183.

Kokkinopoulos, I., Ishida, H., Saba, R., Coppen, S., Suzuki, K. and Yashiro, K. (2016). Cardiomyocyte Differentiation From Mouse Embryonic Stem Cells Using a Simple and Defined Protocol. *Dev Dyn* 157–165.

Kurek, D., Neagu, A., Tastemel, M., Tüysüz, N., Lehmann, J., Van De Werken, H. J. G., Philipsen, S., Van Der Linden, R., Maas, A., Van Ijcken, W. F. J., et al. (2015). Endogenous WNT signals mediate BMP-induced and spontaneous differentiation of epiblast stem cells and human embryonic stem cells. *Stem Cell Reports* **4**, 114–128.

L'Honore, A., Ouimette, J. F., Lavertu-Jolin, M. and Drouin, J. (2010). Pitx2 defines alternate pathways acting through MyoD during limb and somitic myogenesis. *Development* **137**, 3847–3856.

Lolas, M., Valenzuela, P. D. T., Tjian, R. and Liu, Z. (2014). Charting Brachyury-mediated developmental pathways during early mouse embryogenesis. *Proc. Natl. Acad. Sci. U. S. A.* **111**, 4478–83.

Mendjan, S., Mascetti, V. L., Ortmann, D., Ortiz, M., Karjosukarso, D. W., Ng, Y., Moreau, T. and Pedersen, R. A. (2014). NANOG and CDX2 Pattern Distinct Subtypes of Human Mesoderm during Exit from Pluripotency. *Cell Stem Cell* 1–16.

Muzumdar, M. D., Tasic, B., Miyamichi, K., Li, L. and Luo, L. (2007). A global double-fluorescent Cre reporter mouse. *Genesis* **45**, 593–605.

Rayon, T., Menchero, S., Nieto, A., Xenopoulos, P., Crespo, M., Cockburn, K., Cañon, S., Sasaki, H., Hadjantonakis, A. K., de la Pompa, J. L., et al. (2014). Notch and Hippo Converge on Cdx2 to Specify the Trophectoderm Lineage in the Mouse Blastocyst. *Dev. Cell* **30**, 410–422.

Saga, Y., Miyagawa-Tomita, S., Takagi, a, Kitajima, S., Miyazaki, J. I. and Inoue, T. (1999). MesP1 is expressed in the heart precursor cells and required for the formation of a single heart tube. *Development* **126**, 3437–47.

Sambasivan, R., Gayraud-Morel, B., Dumas, G., Cimper, C., Paisant, S., Kelly, R. G. and Tajbakhsh, S. (2009). Distinct regulatory cascades govern extraocular and pharyngeal arch muscle progenitor cell fates. *Dev Cell* **16**, 810–821.

Shedlovsky, A., King, T. R. and Dove, W. F. (1988). Saturation germ line mutagenesis of the murine t region including a lethal allele at the quaking locus. *Proc Natl Acad Sci U S A* **85**, 180–184.

Shelton, M., Metz, J., Liu, J., Carpenedo, R. L., Demers, S. P., Stanford, W. L. and Skerjanc, I. S. (2014). Derivation and expansion of PAX7-positive muscle progenitors from human and mouse embryonic stem cells. *Stem Cell Reports* **3**, 516–529.

Tajbakhsh, S., Rocancourt, D., Cossu, G. and Buckingham, M. (1997). Redefining the genetic hierarchies controlling skeletal myogenesis: Pax-3 and Myf-5 act upstream of MyoD. *Cell* **89**, 127–138.

Tzouanacou, E., Wegener, A., Wymeersch, F. J., Wilson, V. and Nicolas, J.-F. (2009). Redefining the progression of lineage segregations during mammalian embryogenesis by clonal analysis. *Dev. Cell* **17**, 365–76.

Vallier, L. and Pedersen, R. A. (2008). Differentiation of Human Embryonic Stem Cells in Adherent and in Chemically Defined Culture Conditions. In *Current Protocols in Stem Cell Biology*, p. 4:1D.4.1-1D.4.7.